

Spectral Properties of Two Coupled Fibonacci Chains

Anouar Moustaj*,¹ Malte Röntgen*,² Christian V. Morfonios,² Peter Schmelcher,^{2,3} and Cristiane Morais Smith¹

¹*Institute of Theoretical Physics, Utrecht University,
Princetonplein 5, 3584CC Utrecht, The Netherlands*

²*Zentrum für Optische Quantentechnologien, Fachbereich Physik,
Universität Hamburg, Luruper Chaussee 149, 22761 Hamburg, Germany*

³*The Hamburg Centre for Ultrafast Imaging, Universität Hamburg,
Luruper Chaussee 149, 22761 Hamburg, Germany*

(Dated: August 11, 2022)

The Fibonacci chain, i.e., a tight-binding model where couplings and/or on-site potentials can take only two different values distributed according to the Fibonacci word, is a classical example of a one-dimensional quasicrystal. With its many intriguing properties, such as a fractal eigenvalue spectrum, the Fibonacci chain offers a rich platform to investigate many of the effects that occur in three-dimensional quasicrystals. In this work, we study the eigenvalues and eigenstates of two identical Fibonacci chains coupled to each other in different ways. We find that this setup allows for a rich variety of effects. Depending on the coupling scheme used, the resulting system (i) possesses an eigenvalue spectrum featuring a richer hierarchical structure compared to the spectrum of a single Fibonacci chain, (ii) shows a coexistence of Bloch and critical eigenstates, or (iii) possesses a large number of degenerate eigenstates, each of which is perfectly localized on only four sites of the system. If additionally, the system is infinitely extended, the macroscopic number of perfectly localized eigenstates induces a perfectly flat quasi band. Especially the second case is interesting from an application perspective, since eigenstates that are of Bloch or of critical character feature largely different transport properties. At the same time, the proposed setup allows for an experimental realization, e.g., with evanescently coupled waveguides or by patterning an anti-lattice with adatoms on a metallic substrate.

I. INTRODUCTION

Aperiodic structures, in particular quasicrystals [1], have attracted the attention of researchers for many decades [2–6]. Even the simplest quasiperiodic, one-dimensional models exhibit a rich variety of behaviour, ranging from critical eigenstate localization properties, through to the appearance of energy spectra that sometimes form a fractal set [7]. The tools used to understand these behaviors include, but are not limited to, renormalization procedures, multifractal analysis, or symmetry considerations [8–10]. One of the peculiar features that these systems show is a hierarchical structure of energy gaps[9]. This gives rise to spectral measures that are singular continuous, such as the fractal set observed in the Fibonacci quasicrystal [6]. This is a feature that was linked to all the critical localization properties observed in quasicrystals as well as other systems that possess some type of aperiodic order [7].

Although the behavior of aperiodic chains has been investigated extensively and in great detail, comparatively little work has been dedicated to the case where two or more chains are coupled to each other, forming an *aperiodic ladder* [11–15]. In this work, we take a step into this realm by analyzing a range of different coupling schemes between two identical one-dimensional Fibonacci chains. Specifically, we study cases where the two chains are directly coupled in a uniform, non-uniform, or quasiperiodic manner, and evaluate the resulting spectral properties, namely the energy eigenvalues and eigenstates. Additionally, we

study a special case of an indirect coupling, that is, two chains coupled to each other through some intermediate sites. These cases are easily tractable, since they possess a reflection symmetry which allows to block-diagonalize the Hamiltonian.

We find different spectra depending on the setup. In the case of uniform coupling, the eigenvalue spectrum is identical to that of two uncoupled Fibonacci chains, but with shifted energy eigenvalues. On the other hand, if the two chains are coupled only through a single site, the spectrum consists of two Fibonacci chains with an on-site defect. The structure of the eigenvalue spectrum becomes more complex for the case of quasiperiodic coupling, for which a richer hierarchical structure reveals itself through a perturbative renormalization approach. If only the sites of one specific type (A or B) are coupled to each other, we show that, for a specific value of the interchain coupling, half of the eigenstates are critical, while the other half are extended. Interestingly, these two different classes of eigenstates possess different parity with respect to a corresponding reflection operation and can thus be selectively excited by incoming waves of negative or positive parity. This could be used to control the transport properties of this system. Finally, we also realise couplings between the chains through some intermediate sites. This leads to the appearance of flat bands in a quasiperiodic lattice.

This paper is organized as follows. To be self-contained, we start by briefly reviewing the properties of the Fibonacci chain in Section II. In Section III, we analyze the simplest way of coupling two Fibonacci chains, namely a uniform one. In Section IV,

we investigate different cases of non-uniform coupling. We start by connecting only sites of a specific type to each other in Section IV A. Then, in Section IV B, we analyze the case where only two sites are coupled. In Section V, we couple the two chains in a quasiperiodic fashion and analyze the resulting eigenvalue spectrum in terms of a renormalization scheme. Finally, in Section VI, we consider the scenario where the two chains are not directly coupled to each other, but through intermediate sites. Our conclusions are presented in Section VII.

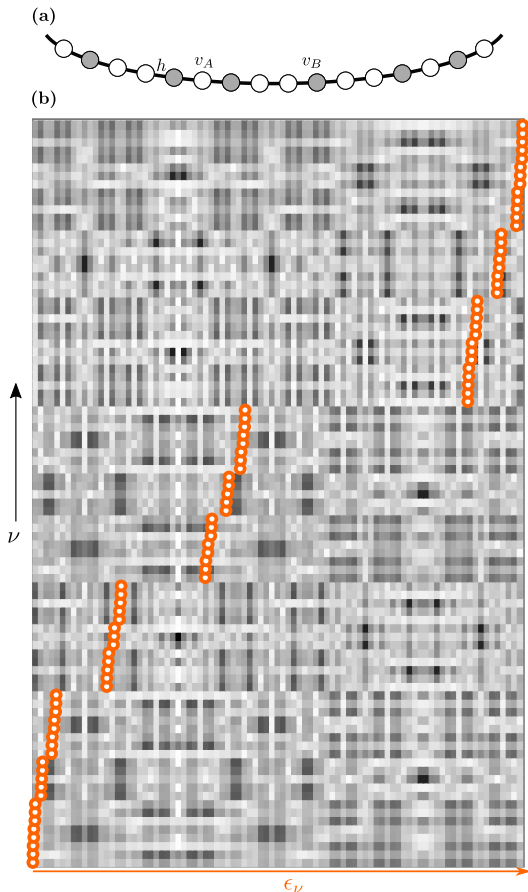


FIG. 1. (a) Graphical representation of a Fibonacci chain with periodic boundary conditions (see text for details). (b) Eigenstate map for such a Fibonacci chain of $N = 89$ sites. Each of the N rows of the gray scale image shows the value of $|\Psi^{(\nu)}(j)|^{1/2}$, where j is a site index, ν is an energy index, and with each square pixel corresponding to one of the N sites. The orange dots denote the eigenenergy ϵ_ν of the eigenstates. The eigenvalues and eigenstates were obtained with $h = -1$, $v_A = 0$ and $v_B = 3$.

II. A SINGLE FIBONACCI CHAIN

We consider a general Fibonacci chain model, namely a nearest-neighbour tight-binding chain with periodic boundary conditions, so that the chain effectively becomes a ring. The on-site potential and hopping

amplitudes are both modulated by the Fibonacci sequence, and the corresponding Hamiltonian is given by

$$H_F = \sum_{i=1}^N v_i |i\rangle \langle i| + \sum_{\langle i,j \rangle} h_i |i\rangle \langle j| \quad (1)$$

where $|i\rangle$ denotes a one-particle quantum state fully localized on the i -th site and $\langle i,j \rangle$ denotes nearest-neighbors. The on-site potential v_i and the hopping amplitude h_i are both binary and follow the sequence of a Fibonacci word S_n of generation n . The latter is defined by the recursion relation

$$S_n = S_{n-1}S_{n-2}, \quad n \geq 2,$$

which is a binary representation of the Fibonacci sequence. This inductive recursion formula is expressed as a string concatenation instead of number addition. Another typical representation is through the substitution rule $A \rightarrow AB$ and $B \rightarrow A$. With the initial two words being $S_0 = B$, $S_1 = A$, the first few words are thus

$$\begin{aligned} S_0 &= B \\ S_1 &= A \\ S_2 &= AB \\ S_3 &= ABA \\ S_4 &= ABAAB \\ S_5 &= ABAABABA \\ S_6 &= ABAABABAABAAB. \end{aligned}$$

We note that the Fibonacci sequence is most commonly represented in numeric form through the recursion formula

$$F_n = F_{n-1} + F_{n-2}, \quad n \geq 2,$$

where $F_0 = F_1 = 1$ and F_n is the n^{th} Fibonacci number, which is equal to the word length $|S_n| = F_n$. Another important property of the sequence is that, in the thermodynamic limit, the ratio between the amount of letters A and B is equal to the golden ratio ϕ . This is more appropriately expressed as [16]

$$\lim_{n \rightarrow \infty} \frac{F_n}{F_{n-1}} = \frac{1 + \sqrt{5}}{2} \equiv \phi.$$

The Hamiltonian (1) can be studied in its general form or reduced to a purely on-site or hopping Fibonacci model, where the parameters $h_i = h$ or $v_i = v$ are uniform. These have been termed diagonal and off-diagonal models in the literature, while Eq. (1) is referred to as the mixed model. All these models have been studied previously in their various forms [17–20], but one important aspect is the equivalence between the on-site and hopping models under a perturbative renormalization scheme [18]. This means that we can uncover all essential features by

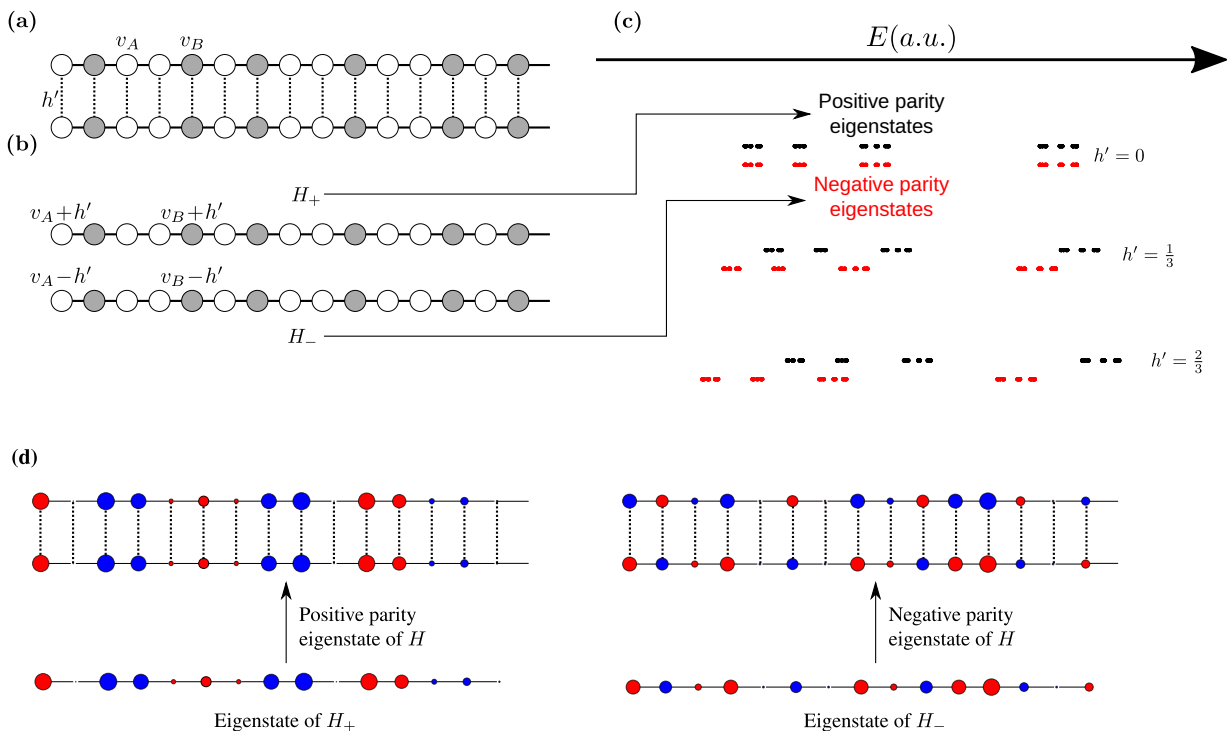


FIG. 2. (a) Two uniformly coupled Fibonacci chains. (b) The result of writing the original system in terms of the symmetry-adapted basis Eqs. (4) and (5). In this basis, the setup decomposes into the two disconnected chains H_+ and H_- . (c) A sketch of the shifting spectra for different coupling strengths h' (see text for details). The eigenstates of H_+ and H_- correspond to eigenstates of the full Hamiltonian H with positive and negative parity, respectively represented in (d). Here, specific eigenstates of H_+ and H_- are shown. At each site, the sign of the eigenstate is represented by a red/blue color, while the amplitude is depicted by the radius of a circle.

studying the unmixed models. For this reason, we will focus on the on-site model for our analysis. In this case, the on-site potential v_i of the i -th site is equal to either v_A or to v_B , depending on whether the i -th character of S_n is equal to A or to B , and the hopping parameter is constant and equal to h . We note that the number of sites in the chain is then equal to $|S_n| = F_n$. Figure 1 (a) shows a graphical representation of such a Fibonacci chain. Due to the periodic boundary conditions, the depicted system constitutes the unit cell of a periodic approximant of the quasicrystal (if $N \rightarrow \infty$, it becomes a proper quasicrystal). This is a system which has long-range order, without being periodic. Its eigenstates form a set of critical states, which have atypical localization properties. This means that they are neither extended nor localized [7]. The eigenvalues have a spectral measure that is singular continuous and form a fractal set (a Cantor set of measure zero). This feature is also observed in the eigenstates, with wavefunctions that show multifractal properties [10]. In Figure 1 (b), the eigenstates of a Fibonacci chain with $N = 89$ are graphically depicted.

The properties of quasicrystals have been studied in a multitude of ways, ranging from perturbative methods based on a renormalization formalism [9, 18] to exact results using a transfer matrix approach [21]

or a symmetry perspective, which offers insights on the fragmentation of states in terms of local spatial structures of the chain [22].

III. UNIFORM COUPLING

Let us investigate the setups where two such chains—each consisting of N sites and with periodic boundary conditions—are coupled to each other in different ways. We will focus on the impact of these different coupling schemes on the corresponding spectral properties.

The first and simplest scenario occurs when the two chains are uniformly coupled to each other, as shown in Fig. 2 (a). The setup is then described by

$$H = H_I + h' \sum_{i=1}^N \left(|i_u\rangle \langle i_l| + |i_l\rangle \langle i_u| \right) \quad (2)$$

with

$$H_I = \sum_{x=u,l} \sum_{i=1}^N v_i |i_x\rangle \langle i_x| + h \sum_{x=u,l} \sum_{\langle i,j \rangle} |i_x\rangle \langle j_x| \quad (3)$$

where $|i_u\rangle$, $|i_l\rangle$ denote one-particle quantum states fully localized on the i -th site of the upper or lower

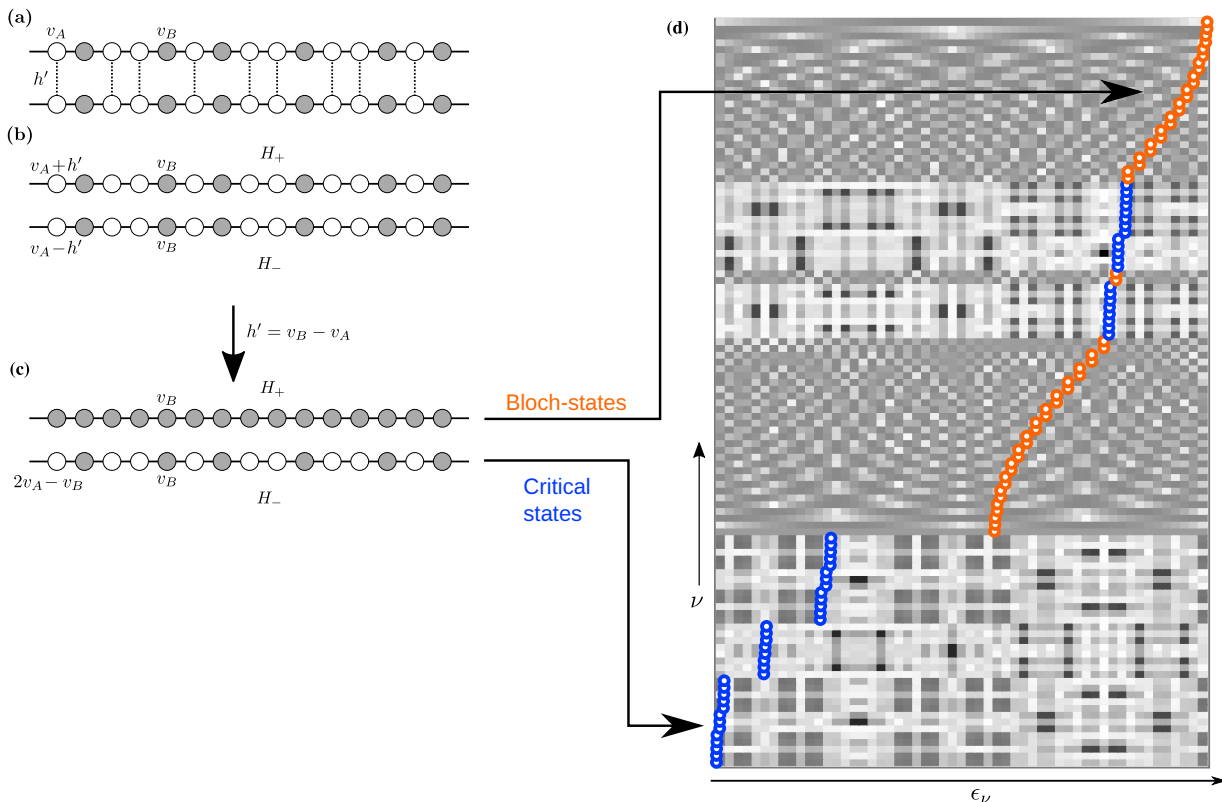


FIG. 3. (a) Two Fibonacci chains that are coupled by connecting their A -sites to each other through couplings with strength h' . (b) The decomposition into H_+ and H_- . (c) When choosing $h' = v_B - v_A$, H_+ becomes periodic, while H_- remains a Fibonacci chain. Thus, the positive parity eigenstates of H (which correspond to symmetrized eigenstates of H_+) are of Bloch-character, while the negative parity eigenstates of H (which correspond to anti-symmetrized eigenstates of H_-) are critical states. (d) The eigenstate map of the setup for this particular choice of h' . Since the eigenstates of H are either symmetric (orange dots; Bloch-states) or anti-symmetric (blue dots; critical states), each of the $2N$ rows in this eigenstate map only shows the amplitudes on one half of the sites of the total system; the full eigenstate could be obtained through symmetrization or anti-symmetrization. The eigenvalues and eigenstates were obtained for $h = -1$, $v_a = 0$ and $v_B = 3$.

chain, respectively. We note that such a setup has been investigated in Ref.[23], though with a focus on the density of states and not on the eigenvalues and eigenstates.

To understand the impact of such a uniform coupling, we employ the up/down mirror symmetry of the setup. Due to this symmetry, the eigenstates have definite parity under an exchange of the lower and upper chain. This fact can be used to construct a symmetry-adapted basis \mathcal{S} , consisting of N states of positive parity

$$|1_u\rangle + |1_l\rangle, \dots, |N_u\rangle + |N_l\rangle \quad (4)$$

and N states with negative parity

$$|1_u\rangle - |1_l\rangle, \dots, |N_u\rangle - |N_l\rangle. \quad (5)$$

Written in this basis, $H' = \mathcal{S}^{-1}H\mathcal{S}$ consists of two isolated subsystems, H_+ and H_- . These two subsystems are shown in Fig. 2 (b). It can be seen that each of them is equal to an isolated Fibonacci chain of N sites, though with on-site potentials uniformly shifted by an amount of plus or minus h' . That is, $H_{\pm} = H_I \pm h'I$, with I being the identity matrix.

Let us now explore the implications of the above, starting with the eigenvalues of H . Since H and H' are related by a similarity transformation, the two Hamiltonians share the same eigenvalue spectrum. Moreover, since H' consists of the two disconnected chains H_{\pm} , the eigenvalue spectrum of H' , $\sigma(H') = \sigma(H)$, is given by the combination of the eigenvalue spectra of these chains [24]. Now, because $H_{\pm} = H_I \pm h'I$, we see that the eigenvalue spectrum of H_+ (H_-) is that of H_I shifted upwards (downwards) by h' , respectively. In other words, the inter-chain coupling strength h' plays the role of an “energy shift parameter” [see Fig. 2 (c)]. Before we continue, we remark that the eigenstates of H can be simply constructed from those of H_+ and H_- by symmetrizing or anti-symmetrizing these states; this is represented in Fig. 2 (d).

IV. NON-UNIFORM COUPLING

Having understood the impact of coupling the two chains uniformly, we now proceed to more complex

scenarios. In all cases, we will maintain the reflection symmetry between the two chains. Thus, we can still decompose the total Hamiltonian into two smaller chains H_+ and H_- .

A. Coupling only A or only B -sites

In the first case, we couple only the A sites to each other, as depicted in Fig. 3(a). Repeating the same steps as above, we obtain $H' = S^{-1}HS = H_+ \oplus H_-$, though now with

$$H_{\pm} = \sum_{i=1}^N v_i^{\pm} |i\rangle \langle i| + h \sum_{\langle i,j \rangle} |i\rangle \langle j| \quad (6)$$

where $v_A^{\pm} = v_A \pm h'$, while $v_B^{\pm} = v_B$ is unchanged [see Fig. 3(b)]. In a completely analogous manner, coupling only the B -sites to each other will result in an energy shift of the on-site potentials of the B -sites only.

A particularly interesting case occurs when coupling only the A -sites and setting $h' = v_B - v_A$. For this special choice of h' , H_+ becomes a uniform chain with zero on-site potential. However, H_- is still a Fibonacci chain. Now, since the eigenstates of H_{\pm} correspond to positive/negative parity eigenstates of the full chain, the system features an interesting combination of traits: while the positive parity eigenstates are *extended*, the negative parity eigenstates are *critical*. This means that the phase diagram of such a Hamiltonian features a special point $h' = v_B - v_A$, at which the system's behavior is highly dependent on the energies of one-particle excitations. As depicted in Fig. 3(a), depending on the energy of these parity eigenstates, they will either form Bloch waves (orange energy levels), or critical states (blue energy levels). It is interesting to see that a specific point in parameter space shows a mixture of singular continuous and absolutely continuous spectra. This provides a platform where both properties of extended and critical states can be exploited by tuning the Fermi level. In the critical regime, for example, (thermal) conductivities are in general very low (in some cases, they are even lower than for conventional insulators) [25, 26]. On the other hand, the fully extended regime provides the possibility to have phases with high (electrical) conductivities.

Finally, let us note that the possibility of Bloch-states in coupled aperiodic setups has also been observed in Refs. [12, 13], in which more complicated coupling schemes have been used.

B. Defect-coupling

Another possibility is the selective coupling of only a small subset of sites. In the extreme case, this subset consists of one site in each chain [see Fig. 4 (a)]. The result of such a coupling can be easily deduced. Using

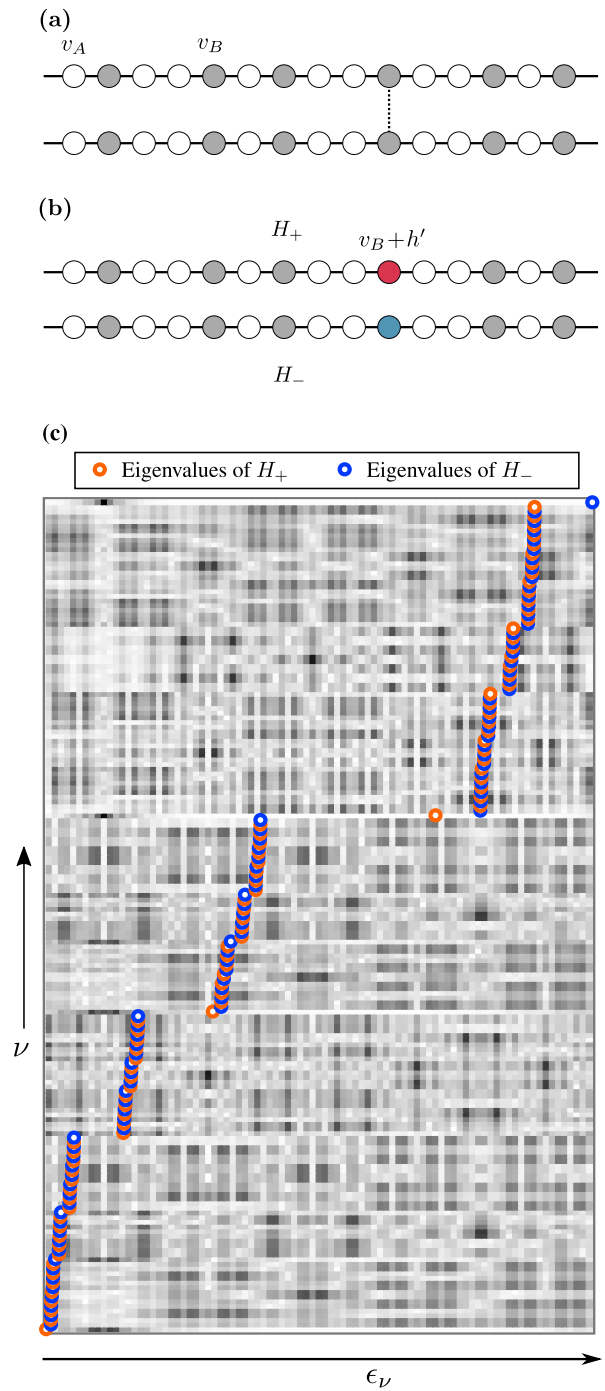


FIG. 4. (a) Two Fibonacci chains coupled by connecting a single site of each chain to each other. (b) The decomposition into H_+ and H_- . (c) Eigenstate map for a setup of two Fibonacci chains that are coupled together at the 10-th site. As a result of this *defect-coupling* (see text for details), several eigenstates lie in gaps between quasi bands. Orange dots correspond to eigenvalues of H_+ and blue dots to those of H_- . The eigenvalues and eigenstates were obtained with $h = -1$, $v_A = 0$ and $v_B = 3$.

the symmetry adapted basis, we see that H_{\pm} will both be simple Fibonacci chains, with added impurities at the

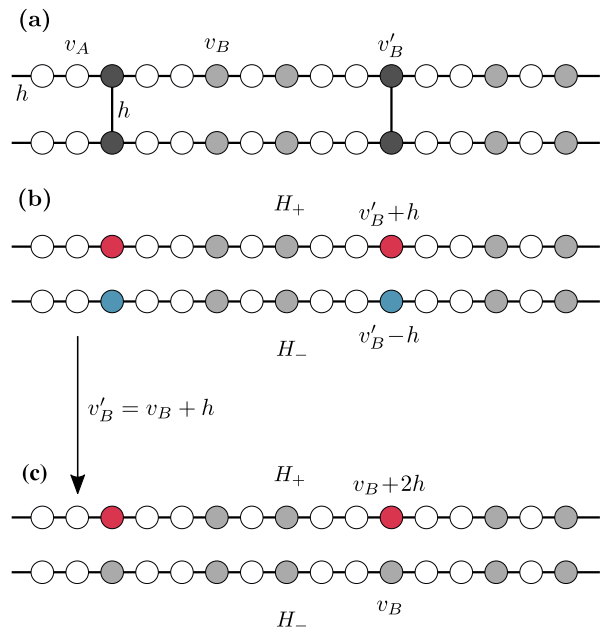


FIG. 5. (a) An excerpt of two Fibonacci chains coupled to each other in quasiperiodic manner, that is, by coupling the B -sites occurring in the pattern $AABAA$ together. (b) The result of the symmetry-induced decomposition into H_+ and H_- . (c) Since we know that the symmetry-induced decomposition results in a different on-site potential for H_{\pm} , we already assign a different v'_B to the coupled sites, which for ease of analysis is set to $v'_B = v_B + h$, resulting in the case we study in more detail in Section V A. In this simplified version, H_- is the standard Fibonacci chain, so we only need to analyze H_+ .

sites that are coupled [see Fig. 4 (b)]. Such systems have been analyzed previously, and it was found that a single weak impurity is sufficient to render the spectrum unstable and reduce its fractal dimension, leading to a loss of criticality in all states [27]. On top of that, it was also recently found that this does not affect all states equally. Using Niu's renormalization procedure [9, 28], it was shown that the degree of criticality loss is dependent on the renormalization path of the site at which the impurity is placed [29]. This means that the location of the impurity impacts which states of the unperturbed Fibonacci chain are the most affected.

Alternatively, the impact of a single-site defect can be analyzed in a framework of local resonators [22]. These local resonators form building blocks of the whole chain. In an unperturbed (without impurity) chain, each eigenstate is approximately symmetric with respect to a local parity operator. The sites with the highest amplitudes will be the ones corresponding to the resonator structures, which are symmetric under local parity. This approximate symmetry depends on the contrast $c = |h|/|v_A - v_B|$, and is exact in the limit $c \rightarrow 0$. By placing an impurity on a particular site, one creates a new local resonator structure in the chain, and as such, new localization properties arise, yielding states

with amplitude distributions that are radically different from the rest of the eigenstates. This can be seen in Fig. 4 (c), where the in-gap states have very strong localization, marked by the darker patches around a particular region of the chain (see the topmost level, for example, where there is a very dark patch around site $j = 10$) around this new local resonator block [22].

V. QUASIPERIODIC COUPLING

Yet another alternative way of coupling the two chains is in a quasiperiodic manner. Out of the many possibilities, here we illustrate an immediate and interesting one: We couple only a subset of B -sites to each other; namely, those appearing in the pattern $AABAA$, as shown in Fig. 5(a), where the darker B site sits in between two A sites on each side. We further set the coupling between the chains to h and choose the coupled B site energy to $v'_B = v_B + h$, such that H_- becomes a regular Fibonacci chain, with on-site energies v_A and v_B . On the other hand, H_+ now features new on-site energies: $v_B + 2h$, distributed in a quasiperiodic manner. For this choice of coupling, there are F_{N-5} such new sites (which is the number of $AABAA$ blocks in a chain of length F_N). Now, we analyze this effective chain using a renormalization approach. Throughout the next subsection, we will assume that $h < 0$ and $v_A < v_B$ to simplify the discussion (see Appendix A for details).

A. Decimation Procedure.

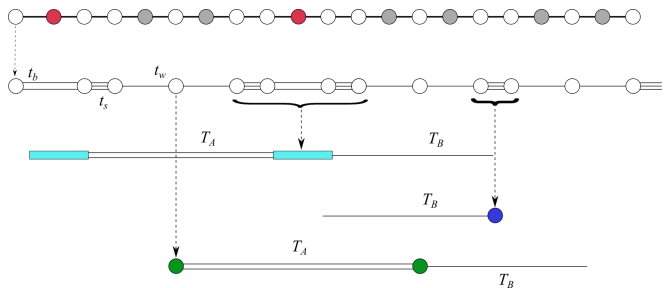


FIG. 6. Decimation procedure for the effective chain described by H_+ . For each of the three degenerate levels, we define a decimated chain with effective new couplings. This allows us to track how the different levels structure themselves. In this example, we focus on the chain resulting from the v_A cluster. The couplings are first renormalized to three values $|t_s| > |t_b| > |t_w|$. The amount of lines connecting the unperturbed eigenstates are representative of the coupling strengths. At the next order of perturbation theory, the unperturbed degenerate eigenstates are slightly more complicated, and correspond to four-atom molecules, dimers, and isolated sites. These then correspond to three chains with cyan, blue and green sites, respectively. The next corrections correspond to the Fibonacci case, where the levels trifurcate at each step.

We can apply the usual decimation procedure known for hierarchical chains [18]. In this case, the novelty lies in the chain with three different on-site energies, as shown for example in Fig. 6. There are three renormalized chains that result from the first decimation step. We can analyze them separately to see how each energy level splits into different branches. A sketch of the branching structure is shown in Fig. 7, where one sees that there are three main clusters. The v_C cluster follows the Fibonacci trifurcating structure from the start. The v_B cluster splits into six levels, each of which starts trifurcating according to the Fibonacci structure. Finally, the v_A cluster splits into seven levels that also trifurcate afterwards. In the thermodynamic limit, these levels keep on trifurcating indefinitely, leading to a spectrum that is a Cantor set and hence, singular continuous. The details of the renormalization procedure can be found in Appendix A. In the next section, we show that these analytic tools lead to a good approximation and understanding of the structure of the spectrum.

B. Effective Couplings and Energy Corrections

In order to calculate the effective couplings and energy corrections at each splitting, we use the Brioullin-Wigner perturbation theory. For each cluster, we use the effective

Hamiltonian [28]

$$H_{\text{eff}} = H_0 + QH_1Q + QH_1P[(E - H_0) - PH_1P]^{-1}PH_1Q, \quad (7)$$

where H_1 is the perturbation corresponding to the weakest coupling, Q is the projector onto the eigenspace of H_0 corresponding to the cluster of interest, while P projects out of it. At first, H_0 is just composed of on-site energies and H_1 of the coupling h between the isolated sites. This results in the three degenerate levels that form the main clusters. In the next order of perturbation theory, H_0 denotes the Hamiltonian of the corresponding renormalized chain, with the weakest coupling turned off. H_1 is then the perturbation with either t_w or t_b turned on, depending on which subchain we are dealing with (i.e. depending on whether $t_b > t_w$ or vice-versa). The details of the next orders that lead to the full Fibonacci structure can be found in Appendix A. Using the Neumann series for the inverse operator [30], we can write the Hamiltonian in terms of powers of H_1 :

$$H_{\text{eff}} = H_0 + QH_1Q + QH_1P \sum_{j=0}^{\infty} [[E - H_0]^{-1}PH_1P]^j [E - H_0]^{-1}PH_1Q.$$

With this effective Hamiltonian for each of the clusters, the renormalized couplings can be found by calculating $\langle E_j | H_{\text{eff}} | E_{j+1} \rangle$, where $|E_j\rangle$ are the zeroth order local eigenstates, which are either one atomic site, a two or a four-atom molecule, depending on the situation. We find the first three renormalized couplings to be given by

$$(t_b, t_s, t_w) = \begin{cases} \left(\frac{c}{1-2c}, 1, c \right) h, & \text{(Cluster A)} \\ \left(-\frac{c^4}{2}, -c, c^2 \right) h, & \text{(Cluster B)} \\ \left(0, -\frac{1}{4} \left[\frac{c}{1-2c} \right]^5, \left[\frac{c}{1-2c} \right]^8 \right) h, & \text{(Cluster C)} \end{cases} \quad (8)$$

where we have defined the contrast parameter $c \equiv |h/(v_A - v_B)|$, which controls how well the perturbation theory behaves. We point out that the physics described by the theory is consistent for

$$c < \frac{1}{4^{\frac{1}{3}}(1 + 4^{\frac{1}{6}})} \approx 0.27875, \quad (9)$$

after which it fails to deliver reasonable results (see Appendix A for more details). We also determined the first-order energy corrections using the same perturbation theory, and found the spectrum shown in

Fig. 8. The energy levels calculated using perturbation theory (in blue) and those from numerical direct diagonalization (in red) have the same structure, with some discrepancies that disappear as the contrast $c \rightarrow 0$. This is illustrated in Fig. 8 (a) and (b) with $c = 1/4$ and $c = 1/8$, respectively. The structure of the spectrum is well approximated by the theory, even for a small chain size of 21 sites. Now, one only needs to add the spectrum of the regular chain to this “modified” chain to obtain the full spectrum of the two connected chains, as shown in Fig. 9. The detailed energy correction formulae can be

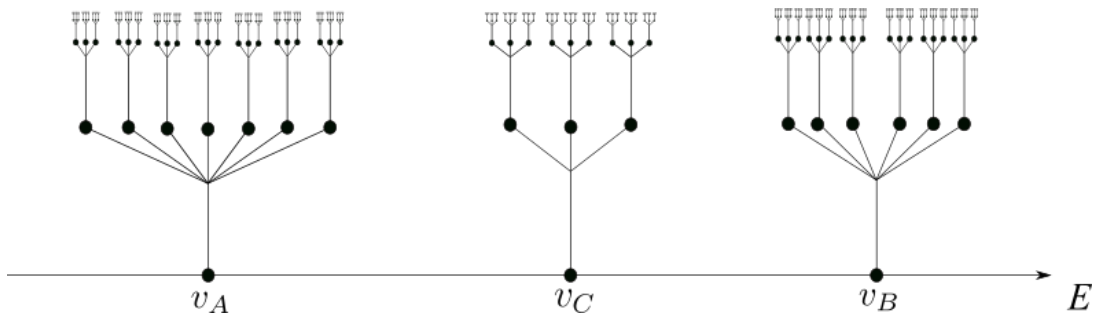


FIG. 7. Energy splitting structure after each renormalization step. Energy scales are greatly distorted and do not represent actual gap sizes. Note that $v_C = v_B + 2h$.

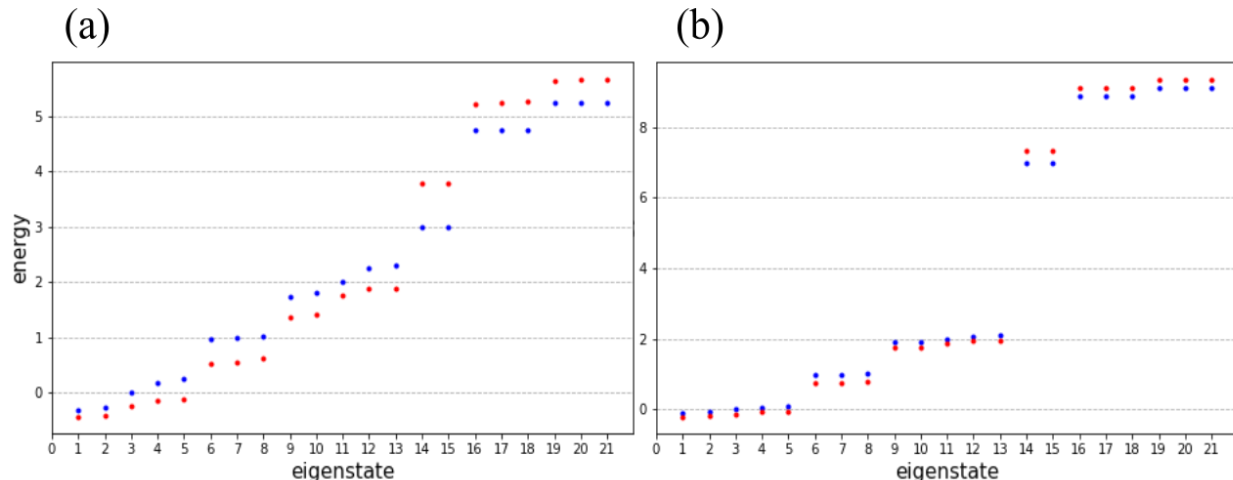


FIG. 8. Comparison between the theoretical framework (blue) and the direct numerical calculation (red) of the chain containing two “impurities” of strength $V_B + 2h$, at the center of the resonator structure $AABAA$. The chain’s length is 21 sites. The structure is the same and the discrepancy gets as smaller as the contrast decreases. (a) Contrast $c = 1/4$, which is close to the limits of applicability of the perturbation theory. (b) Contrast $c = 1/8$. The energy is shown in arbitrary units.

found in Appendix B.

VI. COUPLING THROUGH INTERMEDIATE SITES

In the following, we consider a case where the two Fibonacci chains are not coupled directly, but instead through intermediate sites. Before we start, let us first investigate a setup where two *periodic* chains are coupled indirectly, as shown in Fig. 10 (a). In Fig. 10 (b), we depict the band structure of this so-called “one-dimensional Lieb lattice” [31]. What makes this lattice interesting is that, among four dispersive bands, it also features one completely flat band fulfilling $E(\mathbf{k}) = \text{constant}$ for all wave vectors \mathbf{k} . This defining feature of flat bands renders them dispersionless; they suppress wave transport [32]. On the other hand, the density of states in a flat band diverges, so that any disorder or non-linear effects may qualitatively change the transport properties [32, 33]. Moreover, in lattices where the

single-particle Hamiltonian features a flat band, even arbitrarily weak interactions may act non-perturbatively. This can lead to boson pair formation [34–36] or other interesting phases, such as the Haldane insulator [37] and Wigner crystals [38].

In two dimensions, a classical example for a system with flat bands is the Lieb lattice, whose structure is very similar to the system depicted in Fig. 10 (a). The two-dimensional Lieb lattice has been realized in a number of different experimental platforms, such as tailored atomic structures on substrates [39, 40], evanescently coupled waveguide arrays [41, 42], terahertz spoof plasmons [43], or cold atom setups [44, 45]. Interestingly, the CuO_2 planes in high-temperature cuprate superconductors possess a Lieb lattice structure, and it has been conjectured that flat bands might play a role in their high critical temperature [32, 46–50].

Flat bands are also interesting from another perspective, since they are tightly connected to the emergence of a special kind of eigenstates, the so-called “compact localized state” (CLS) [51–53]. For the

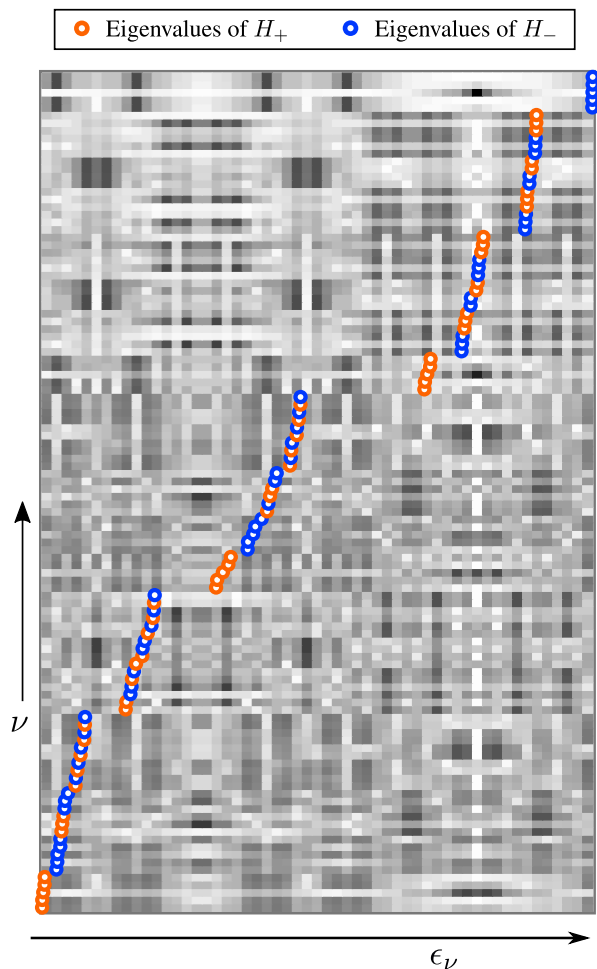


FIG. 9. Eigenstate map for a setup consisting of two quasiperiodically coupled Fibonacci chains, each of length $N = 55$ sites. Orange dots correspond to eigenvalues of H_+ and blue dots correspond to eigenvalues of H_- .

one-dimensional Lieb lattice, a CLS is shown in Fig. 10 (a), consisting of an excitation of only four B sites. The CLS thus “lives” only on a single plaquette (marked by a dotted rectangle) and strictly vanishes outside it. In other words, it is perfectly localized on a very small part of the setup.

The defining feature of CLSs — namely, their perfect localization — renders these states very robust against perturbations: Since they vanish *exactly* outside their localization domain \mathcal{D} , they are not affected by any changes to the system outside \mathcal{D} . Due to this property, CLSs are ideal candidates for storing information [54, 55]. The perfect localization of CLSs might further be interesting in the context of photonic waveguide arrays, where it allows for diffraction-free transmission of information in the form of CLSs [41, 56].

After the above considerations, let us now couple two aperiodic Fibonacci chains in an indirect manner. Out of the many possibilities, here we choose one of the simplest, yet quite interesting setup, depicted in Fig. 10 (c). Each

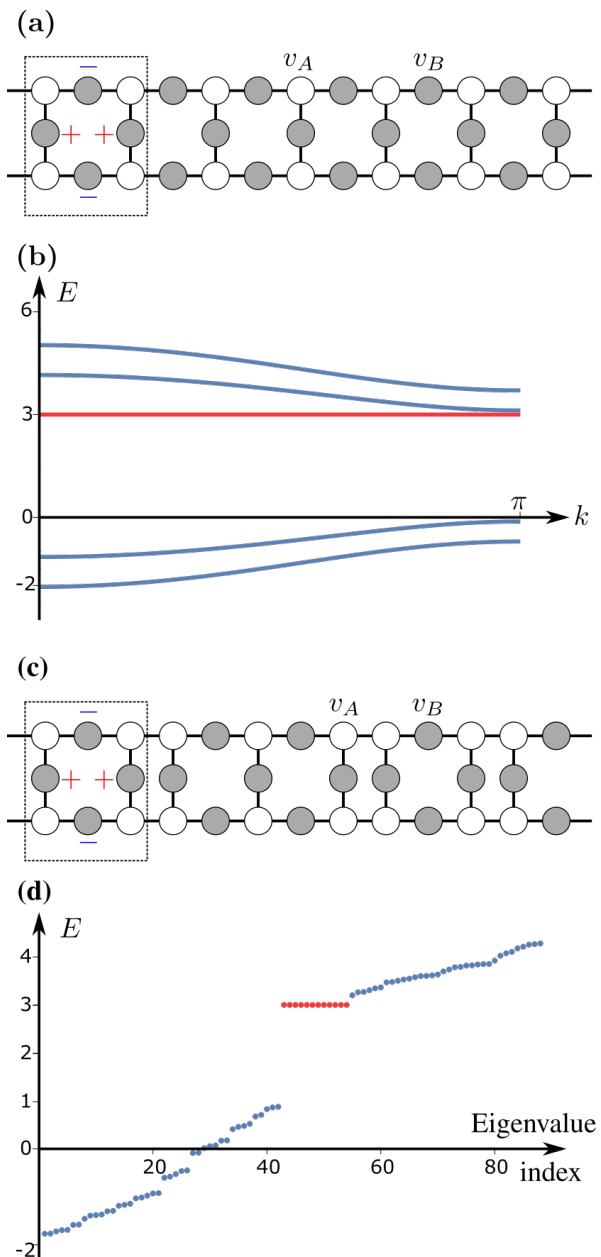


FIG. 10. (a) The one-dimensional Lieb-lattice and its spectrum (b). (c) the quasiperiodic Lieb lattice and its spectrum (d). For the quasiperiodic Lieb lattice, the spectrum was computed for a finite setup with a total number of 88 sites (34 in the upper and lower chain and 20 B -sites in the center). For all figures, $v_A = 0$ and $v_B = h = 1$.

A -site of the upper chain is coupled by an intermediate B -site to its counterpart A -site on the lower chain. This setup also features a macroscopic number of CLSs, one of which is depicted in Fig. 10 (c).

When comparing the one-dimensional version of the Lieb lattice [57, 58]—shown in Fig. 10 (a)—to the coupled Fibonacci chains depicted in Fig. 10 (c), one sees that they are rather similar. Due to this high similarity, we call the coupled Fibonacci setup of Fig. 10

(c) the “quasiperiodic Lieb lattice”. The similarity in the structure of the two lattices is also visible in their eigenvalue spectra, since both lattices feature a flat (quasi) band. The emergence of this flat band can easily be understood, since (for an infinite setup) there is an infinite number of plaquettes, and thus an infinite number of degenerate CLSs. In both cases, the flat bands emerge due to destructive interference [32].

VII. CONCLUSIONS

In this work, we analyzed various ways of coupling two identical Fibonacci chains to each other. The main tool that helped us to identify the features of these systems is a symmetry adapted block-diagonalization of the Hamiltonian H into $H_+ \oplus H_-$. Once we find the eigenstates of H_{\pm} , we can symmetrize/anti-symmetrize them, respectively, to obtain the eigenstates of the original Hamiltonian H . In addition, the eigenvalue spectrum of the system is simply given by a multiset sum of the eigenvalue spectra of the blocks H_{\pm} .

After briefly introducing the individual Fibonacci chain, we started by exploring the effects of uniformly coupling two identical chains. We then found that the resulting eigenvalue spectrum is just a sum of two shifted Fibonacci spectra, which renders the behaviour of a particle in such a system identical to that in a conventional Fibonacci chain. We have subsequently explored the case of a nonuniform coupling, where we coupled only A (or only B) sites. An interesting scenario occurs when the interchain coupling is $h' = v_B - v_A$, since H_+ then becomes a periodic chain, for which the eigenstates are Bloch waves. On the other hand, H_- is still a Fibonacci chain, such that the complete spectrum offers a mixture of critical and fully extended eigenstates, identifiable by the parity of the corresponding wavefunctions. The next type of coupling that we have analyzed is between a small subset of

sites, i.e. a so called defect coupling, leading to block Hamiltonians H_{\pm} which are Fibonacci chains with on-site defects. This has been followed by another interesting and more complicated case of quasiperiodically coupled chains. The resulting block Hamiltonians could be thought to be like several coupled defects, but we have shown, through a perturbative renormalization analysis, that all states in this chain belong to the same family of critical states. Finally, we explored two Fibonacci chains coupled to each other in the same manner as the nonuniform coupling of Section IV, but with an intermediate site in between. This offers the possibility of having a set of CLSs, leading to a flat band in the energy spectrum. Overall, the demonstrated emergence of CLSs in the quasiperiodic Lieb lattice represents an interesting addition to the existing literature on these phenomena in quasiperiodic setups (see, for instance, [59–62]). Two immediate tasks for the near future would be to analyze the quasiperiodic Lieb lattice in the context of interacting electrons, or to investigate the impact of (correlated) disorder on the transport properties.

In summary, we find that the analyzed system of two coupled Fibonacci chains allows for a rich variety of effects, well beyond the already fascinating behavior exhibited by a single chain. As future work, the coexistence extended, localized and critical states might be useful for building electronic devices [14].

ACKNOWLEDGMENTS

This publication is part of the project TOPCORE with project number OCENW.GROOT.2019.048, which is financed by the Dutch Research Council (NWO). This work (P.S.) is supported by the Cluster of Excellence ‘Advanced Imaging of Matter’ of the Deutsche Forschungsgemeinschaft (DFG) - EXC 2056 - project ID 390715994.

* A.M. and M.R. contributed equally to this work.

-
- [1] D. Shechtman, I. Blech, D. Gratias, and J. W. Cahn, Metallic phase with long-range orientational order and no translational symmetry, *Phys. Rev. Lett.* **53**, 1951 (1984).
 - [2] T. Janssen, Crystallography of quasi-crystals, *Act. Crystall. Sect. A* **42**, 261 (1986).
 - [3] C. Berger, T. Grenet, P. Lindqvist, P. Lanco, J. Grieco, G. Fourcaudot, and F. Cyrot-Lackmann, The new alpdre icosahedral phase: Towards universal electronic behaviour for quasicrystals?, *Solid State Communications* **87**, 977 (1993).
 - [4] A. P. Vieira, Low-Energy Properties of Aperiodic Quantum Spin Chains, *Physical Review Letters* **94**, 077201 (2005).
 - [5] D. Tanese, E. Gurevich, F. Baboux, T. Jacqmin, A. Lemaître, E. Galopin, I. Sagnes, A. Amo, J. Bloch, and E. Akkermans, Fractal Energy Spectrum of a Polariton Gas in a Fibonacci Quasiperiodic Potential, *Physical Review Letters* **112**, 146404 (2014).
 - [6] A. Jagannathan, The Fibonacci quasicrystal: Case study of hidden dimensions and multifractality, arXiv:2012.14744 (2021), arXiv:2012.14744.
 - [7] E. Maciá, The role of aperiodic order in science and technology, *Reports on Progress in Physics* **69**, 397 (2005).
 - [8] M. de Boissieu, Ted Janssen and aperiodic crystals, *Act. Crystall. Sect. A* **75(Pt 2)**, 273–280. (2019).
 - [9] Q. Niu and F. Nori, Renormalization-group study of one-dimensional quasiperiodic systems, *Phys. Rev. Lett.* **57**, 2057 (1986).
 - [10] N. Macé, A. Jagannathan, and F. Piéchon, Fractal dimensions of wave functions and local spectral measures on the Fibonacci chain, *Phys. Rev. B* **93**, 205153 (2016).
 - [11] D. A. Moreira, E. L. Albuquerque, and C. G. Bezerra, Specific heat spectra for quasiperiodic ladder sequences,

- The European Physical Journal B **54**, 393 (2006).
- [12] B. Pal and A. Chakrabarti, Absolutely continuous energy bands in the electronic spectrum of quasiperiodic ladder networks, *Physica E: Low-dimensional Systems and Nanostructures* **60**, 188 (2014).
- [13] A. Mukherjee, A. Nandy, and A. Chakrabarti, Controlled delocalization of electronic states in a multi-strand quasiperiodic lattice, *Eur. Phys. J. B* **90**, 52 (2017).
- [14] M. Saha and S. K. Maiti, Particle current rectification in a quasi-periodic double-stranded ladder, *Journal of Physics D: Applied Physics* **52**, 465304 (2019).
- [15] S. Roy, S. K. Maiti, L. M. Pérez, J. H. O. Silva, and D. Laroze, Localization Properties of a Quasiperiodic Ladder under Physical Gain and Loss: Tuning of Critical Points, Mixed-Phase Zone and Mobility Edge, *Materials* **15**, 597 (2022).
- [16] E. Kilic, The binet formula, sums and representations of generalized fibonacci p-numbers, *European Journal of Combinatorics* **29**, 701 (2008).
- [17] C. Sire and R. Mosseri, Excitation spectrum, extended states, gap closing : some exact results for codimension one quasicrystals, *Journal de Physique* **51**, 1569 (1990).
- [18] Q. Niu and F. Nori, Spectral splitting and wave-function scaling in quasicrystalline and hierarchical structures, *Phys. Rev. B* **42**, 10329 (1991).
- [19] M. Kohmoto and J. R. Banavar, Quasiperiodic lattice: Electronic properties, phonon properties, and diffusion, *Phys. Rev. B* **34**, 563 (1986).
- [20] M. Kohmoto, B. Sutherland, and C. Tang, Critical wave functions and a cantor-set spectrum of a one-dimensional quasicrystal model, *Phys. Rev. B* **35**, 1020 (1987).
- [21] M. Kohmoto, L. P. Kadanoff, and C. Tang, Localization problem in one dimension: Mapping and escape, *Phys. Rev. Lett.* **50**, 1870 (1983).
- [22] M. Röntgen, C. V. Morfonios, R. Wang, L. Dal Negro, and P. Schmelcher, Local symmetry theory of resonator structures for the real-space control of edge states in binary aperiodic chains, *Phys. Rev. B* **99**, 214201 (2019).
- [23] E. Lazo, Multifractal Behavior of a Fibonacci Crystal Built over p Coupled Chains, in *Instabilities and Nonequilibrium Structures VI*, Nonlinear Phenomena and Complex Systems, edited by E. Tirapegui, J. Martínez, and R. Tiemann (Springer Netherlands, Dordrecht, 2000) pp. 387–392.
- [24] To be precise, the spectrum of H is the multiset sum of the spectra of H_+ and H_- .
- [25] P. Archambault and C. Janot, Thermal conductivity of quasicrystals and associated processes, *MRS Bulletin* **22**, 48–53 (1997).
- [26] Janot, C., The properties and applications of quasicrystals, *Europhys. News* **27**, 60 (1996).
- [27] G. G. Naumis and J. L. Aragón, Substitutional disorder in a Fibonacci chain: Resonant eigenstates and instability of the spectrum, *Phys. Rev. B* **54**, 15079 (1996).
- [28] Q. Niu and F. Nori, Spectral splitting and wave-function scaling in quasicrystalline and hierarchical structures, *Phys. Rev. B* **42**, 10329 (1990).
- [29] A. Moustaj, S. Kempkes, and C. M. Smith, Effects of disorder in the Fibonacci quasicrystal, *Phys. Rev. B* **104**, 144201 (2021).
- [30] E. Schechter, Chapter 23 - normed operators, in *Handbook of Analysis and Its Foundations*, edited by E. Schechter (Academic Press, San Diego, 1997) pp. 607–628.
- [31] A. Ramachandran, C. Danieli, and S. Flach, Fano resonances in flat band networks, in *Fano Resonances in Optics and Microwaves*, Vol. 219, edited by E. Kamenetskii, A. Sadreev, and A. Miroshnichenko (Springer International Publishing, Cham, 2018) pp. 311–329.
- [32] D. Leykam, A. Andrianov, and S. Flach, Artificial flat band systems: From lattice models to experiments, *Adv. Phys.* **3**, 1473052 (2018).
- [33] D. Leykam, J. D. Bodyfelt, A. S. Desyatnikov, and S. Flach, Localization of weakly disordered flat band states, *Eur. Phys. J. B* **90**, 1 (2017).
- [34] A. Mielke, Pair formation of hard core bosons in flat band systems, *J Stat Phys* **171**, 679 (2018).
- [35] P. Puddleiner and A. Mielke, Interacting bosons in two-dimensional flat band systems, *Eur. Phys. J. B* **88**, 207 (2015).
- [36] S. Takayoshi, H. Katsura, N. Watanabe, and H. Aoki, Phase diagram and pair Tomonaga-Luttinger liquid in a Bose-Hubbard model with flat bands, *Phys. Rev. A* **88**, 063613 (2013).
- [37] B. Grémaud and G. G. Batrouni, Haldane phase on the sawtooth lattice: Edge states, entanglement spectrum, and the flat band, *Phys. Rev. B* **95**, 165131 (2017).
- [38] M. Tovmasyan, *Strongly Correlated Phases in Flatband Lattices*, Ph.D. thesis, ETH Zurich (2018).
- [39] M. R. Slot, T. S. Gardenier, P. H. Jacobse, G. C. P. van Miert, S. N. Kempkes, S. J. M. Zevenhuizen, C. M. Smith, D. Vanmaekelbergh, and I. Swart, Experimental realization and characterization of an electronic Lieb lattice, *Nat. Phys.* **13**, 672 (2017).
- [40] R. Drost, T. Ojanen, A. Harju, and P. Liljeroth, Topological states in engineered atomic lattices, *Nat. Phys.* **13**, 668 (2017).
- [41] R. A. Vicencio, C. Cantillano, L. Morales-Inostroza, B. Real, C. Mejía-Cortés, S. Weimann, A. Szameit, and M. I. Molina, Observation of localized states in lieb photonic lattices, *Phys. Rev. Lett.* **114**, 245503 (2015).
- [42] S. Mukherjee, A. Spracklen, D. Choudhury, N. Goldman, P. Öhberg, E. Andersson, and R. R. Thomson, Observation of a localized flat-band state in a photonic Lieb lattice, *Phys. Rev. Lett.* **114**, 245504 (2015).
- [43] S. Kajiwara, Y. Urade, Y. Nakata, T. Nakanishi, and M. Kitano, Observation of a nonradiative flat band for spoof surface plasmons in a metallic lieb lattice, *Phys. Rev. B* **93**, 075126 (2016).
- [44] S. Taie, T. Ichinose, H. Ozawa, and Y. Takahashi, Spatial adiabatic passage of massive quantum particles in an optical Lieb lattice, *Nat. Commun.* **11**, 257 (2020).
- [45] S. Taie, H. Ozawa, T. Ichinose, T. Nishio, S. Nakajima, and Y. Takahashi, Coherent driving and freezing of bosonic matter wave in an optical lieb lattice, *Sci. Adv.* **1**, e1500854 (2015).
- [46] S. Peotta and P. Törmä, Superfluidity in topologically nontrivial flat bands, *Nat. Commun.* **6**, 8944 (2015).
- [47] A. Julku, S. Peotta, T. I. Vanhala, D.-H. Kim, and P. Törmä, Geometric origin of superfluidity in the Lieb-lattice flat band, *Phys. Rev. Lett.* **117**, 045303 (2016).
- [48] K. Kobayashi, M. Okumura, S. Yamada, M. Machida, and H. Aoki, Superconductivity in repulsively interacting fermions on a diamond chain: Flat-band-induced pairing,

- Phys. Rev. B **94**, 214501 (2016).
- [49] M. Tovmasyan, S. Peotta, P. Törmä, and S. D. Huber, Effective theory and emergent SU(2) symmetry in the flat bands of attractive Hubbard models, Phys. Rev. B **94**, 245149 (2016).
- [50] L. Liang, T. I. Vanhala, S. Peotta, T. Siro, A. Harju, and P. Törmä, Band geometry, Berry curvature, and superfluid weight, Phys. Rev. B **95**, 024515 (2017).
- [51] W. Maimaiti, A. Andreanov, H. C. Park, O. Gendelman, and S. Flach, Compact localized states and flat-band generators in one dimension, Phys. Rev. B **95**, 115135 (2017).
- [52] J.-W. Rhim and B.-J. Yang, Singular flat bands, Adv. Phys. X **6**, 1901606 (2021).
- [53] J.-W. Rhim and B.-J. Yang, Classification of flat bands according to the band-crossing singularity of Bloch wave functions, Phys. Rev. B **99**, 045107 (2019).
- [54] M. Röntgen, C. V. Morfonios, I. Brouzos, F. K. Diakonov, and P. Schmelcher, Quantum network transfer and storage with compact localized states induced by local symmetries, Phys. Rev. Lett. **123**, 080504 (2019).
- [55] S. N. Kempkes, P. Capiod, S. Ismaili, J. Mulkens, I. Swart, and C. M. Smith, Compact localized boundary states in a quasi-1d electronic diamond-necklace chain, arXiv: 2201.02012 (2022).
- [56] R. A. Vicencio and C. Mejía-Cortés, Diffraction-free image transmission in kagome photonic lattices, J. Opt. **16**, 015706 (2013).
- [57] E. H. Lieb, Two theorems on the Hubbard model, Phys. Rev. Lett. **62**, 1201 (1989).
- [58] S. Flach, D. Leykam, J. D. Bodyfelt, P. Matthies, and A. S. Desyatnikov, Detangling flat bands into Fano lattices, Europhys. Lett. **105**, 30001 (2014).
- [59] B. Sutherland, Localization of electronic wave functions due to local topology, Phys. Rev. B **34**, 5208 (1986).
- [60] H. Ha and B.-J. Yang, Macroscopically degenerate localized zero-energy states of quasicrystalline bilayer systems in the strong coupling limit, Phys. Rev. B **104**, 165112 (2021).
- [61] M. Kohmoto and B. Sutherland, Electronic and vibrational modes on a Penrose lattice: Localized states and band structure, Phys. Rev. B **34**, 3849 (1986).
- [62] F. Nori and Q. Niu, Angular momentum irreducible representation and destructive quantum interference for Penrose lattice Hamiltonians, in *Quasicrystals And Incommensurate Structures In Condensed Matter-Proceedings Of The Third International Meeting On Quasicrystals*, Vol. 1001 (World Scientific Publishing Co., Singapore, 1990) p. 434.

Appendix A: Determination of effective hopping amplitudes and energy corrections of the quasiperiodic coupling case

In this appendix, we show the detailed calculations of the renormalized hopping constants. Figure 11 shows that one can form three effective chains (a), (b) and (c), corresponding to the clusters v_A , v_B and $v_C = v_B + 2h$ respectively. Before deriving our results, we recall that we are working in the regime of parameters where $v_A < v_B$ and $h < 0$. This is done to obtain

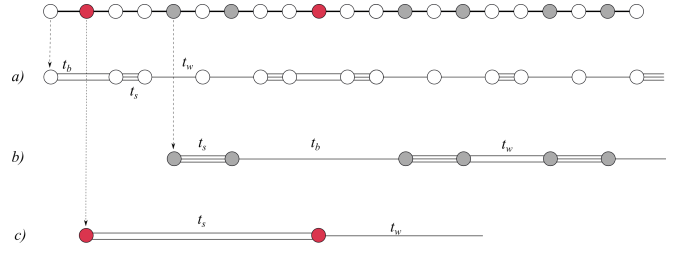


FIG. 11. Decimation procedure. The topmost chain results from the equipartition theorem applied to the coupled Fibonacci chains we started with. It corresponds to the Hamiltonian H_+ with red sites of energies $v_C = v_B + 2h$. The white and grey sites have energies v_A and v_B respectively. (a) The renormalized chain that was shown as an example in Section V, with $|t_s| > |t_b| > |t_w|$. (b) The chain corresponding to the renormalization of the grey sites. In this case, we have $|t_s| > |t_w| > |t_b|$. (c) The chain corresponding to the renormalization of the red sites, with $|t_s| > |t_w|$. This chain is already a proper hopping Fibonacci chain.

a hierarchy of hopping strengths that will result in the infinitely trifurcating structure after (at most) the second renormalization step. The V_C cluster is a regular hopping Fibonacci chain. In fact, if one starts from a chain of generation N , with F_N sites, one ends up with one of generation $N - 5$, with F_{N-5} sites. By calculating the matrix element $\langle E_j | H_{\text{eff}} | E_{j+1} \rangle$, where H_{eff} is given by Eq. (7), between the nearest neighbouring eigenstates of the unperturbed Hamiltonian H_0 in the $E = v_C$ subspace, we find that this chain has effective renormalized hoppings, to nearest order in the contrast $c = |h|/|v_A - v_B|$, given by

$$t_s = \frac{h^6}{4(v_B - v_A + 2h)^5} = -\frac{1}{4} \left[\frac{c}{1 - 2c} \right]^5 h, \quad (\text{A1})$$

$$t_w = \frac{h^9}{(v_B - v_A + 2h)^8} = \left[\frac{c}{1 - 2c} \right]^8 h.$$

Next, we consider the v_B chain, which contains six clusters. Two clusters correspond to the two-atom molecule bonded by t_s , while the other four correspond to the four-atom molecule (composed of two two-atom molecules bonded by $|t_w| > |t_b|$). These clusters will further start to trifurcate because they end up having the structure of a hopping Fibonacci chain after decimation. The renormalized hoppings of this chain are given by

$$t_b = \frac{-h^5}{2(v_B - v_A)^4} = -\frac{c^4}{2} h,$$

$$t_s = \frac{h^2}{v_B - v_A} = -ch, \quad (\text{A2})$$

$$t_w = \frac{h^3}{(v_B - v_A)^2} = c^2 h.$$

Finally, we consider the v_A cluster. It has seven clusters. The six clusters come from the same structures as the v_B chain, i.e two- and four-atoms molecules, and

the additional cluster comes from isolated sites. Once again, each one of these clusters will start trifurcating at the next steps of decimation, and one retrieves the hopping Fibonacci chain structure. The renormalized hoppings of this chain are

$$\begin{aligned} t_b &= \frac{h^2}{v_A - v_B - 2h} = \frac{c}{1 - 2c} h, \\ t_s &= h, \\ t_w &= \frac{h^2}{v_A - v_B} = ch. \end{aligned} \quad (\text{A3})$$

Let us now study the regime of validity which results in the hopping hierarchy discussed previously. Starting with the v_B subspace, which is the simplest to deal with, we see from Eq. (A2) that the hierarchy $|t_s| > |t_w| > |t_b|$ will always hold for $c \in (0, 1)$. This immediately results in the trifurcating structure after one iteration of the renormalization procedure. The v_A subspace, on the other hand, restricts the range of c further. In order to have $|t_s| > |t_b| > |t_w|$, we must impose

$$1 > \left| \frac{c}{1 - 2c} \right| > c$$

which leads to $0 < c < 1/3$. Finally, the v_C subspace will give us the final restriction to impose the hierarchy leading to a trifurcating structure. This means we want $|t_s| > |t_w|$, leading to

$$\frac{1}{4} \left| \frac{c}{1 - 2c} \right|^5 > \left| \frac{c}{1 - 2c} \right|^8$$

Solving for $c > 0$ yields the final restriction

$$c < \frac{1}{4^{\frac{1}{3}}(1 + 4^{\frac{1}{6}})}. \quad (\text{A4})$$

In the next subsections, we will determine the energy corrections and the renormalized Fibonacci hoppings for each cluster.

1. v_A cluster

Starting with the v_A cluster, we can split it into the three categories depicted in Fig. 12. The 4-atom molecule leads to four energy eigenvalues,

$$E_{4M}^A = \pm \frac{1}{\sqrt{2}} \sqrt{t_b^2 + 2t_s^2 \pm \sqrt{(t_b^2 + 2t_s^2)^2 - 4t_s^4}}, \quad (\text{A5})$$

where the subscript $4M$ reminds us that it is for the 4-atom molecule, while the superscript A indicates that it applies to the initial level v_A . The 2-atom molecule and the isolated atom have eigenvalues, respectively, equal to

$$E_{2M}^A = \pm t_s, \quad (\text{A6})$$

$$E_A^A = 0. \quad (\text{A7})$$

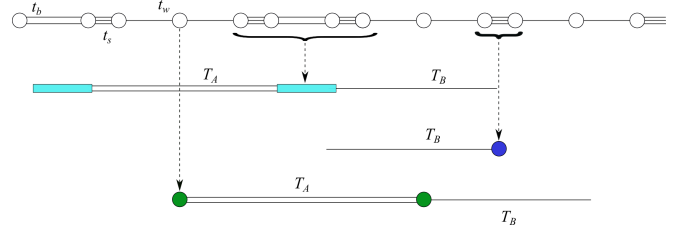


FIG. 12. Decimation of the v_A cluster's effective chain. The cyan rectangles represent the states corresponding to the four-atom molecules. They correspond to the renormalized sites of the chain, and have an on-site energy given by E_{4M} . The effective hoppings T_A and T_B are Fibonacci distributed and further renormalization leads to the Fibonacci trifurcating structure. Below, we have the two-atom molecular chain, where each blue site represents a dimer. In this figure, only one of them appears, but for a larger chain, there are Fibonacci distributed couplings, whence the trifurcating structure starts after this point in the renormalization procedure. Finally, the bottom chain corresponds to isolated (green) sites, forming the last degenerate subspace of H_0^A . The effective chain for this subspace also has couplings that are Fibonacci distributed.

In order to calculate the effective hoppings using the Brillouin-Wigner degenerate perturbation theory, we need to know the eigenstates of H_0^A , which for the $E_A^A = 0$ level are just the corresponding isolated sites. For the 2-atom molecules, these are given by $|E_{2M}^A\rangle = 2^{-1/2}(|i\rangle \pm |i+1\rangle)$ for some localized one-particle state at site number i , corresponding to the sites coupled by the strongest bond, and for the 4-atom molecules

$$|E_{4M}^A\rangle = \frac{a_0|i\rangle + a_1|i+1\rangle + a_2|i+2\rangle + a_3|i+3\rangle}{\sqrt{a_0^2 + a_1^2 + a_2^2 + a_3^2}}$$

for the relevant sites i to $i+3$, as shown in Fig. 12. The coefficients are given by

$$\begin{aligned} a_0 &= 1, & a_1 &= \frac{E_{4M}}{t_s}, \\ a_2 &= \frac{t_b}{t_s} \frac{E_{4M}^2}{E_{4M}^2 - t_s^2}, & a_3 &= \frac{t_b E_{4M}}{E_{4M}^2 - t_s^2}, \end{aligned} \quad (\text{A8})$$

where we omitted the superscript A for brevity. Each of these degenerate subspaces can be associated to its own chain, with its own couplings in the renormalization picture (see Fig. 12).

The effective Hamiltonian for the v_A cluster is found by setting the perturbation Hamiltonian H_1 to be the one with all matrix elements containing t_w . We remind the reader that the general expression was given by Eq. (7).

a. E_{4M} Chain (cyan) The couplings in the 4-atom molecular chain are given by the matrix element $\langle E_{4M,j}^A | H_{eff}^A | E_{4M,j+1}^A \rangle$, where j is the renormalized site

index. To nearest order in t_w , they read

$$\begin{aligned} T_A &= \frac{a_3}{N} \frac{t_w^2}{E_{4M}}, \\ T_B &= \frac{a_3}{N} \frac{t_w^4 t_s}{E_{4M}^2 (E_{4M}^2 - t_s^2)}, \end{aligned} \quad (\text{A9})$$

where we defined $N \equiv a_0^2 + a_1^2 + a_2^2 + a_3^2$. Note that there are four different E_{4M} 's and hence four sets of coefficients a .

b. E_{2M} Chain (blue) The 2-atom molecular chain's couplings are obtained from the matrix elements $\langle E_{2M,j}^A | H_{eff}^A | E_{2M,j+1}^A \rangle$. The calculation yields

$$\begin{aligned} T_A &= \pm \frac{t_w^4}{2t_s^2} \sum_{j=0}^3 \frac{a_3^{(j)}}{N_j (\pm t_s - E_{4M}^{(j)})}, \\ T_B &= \frac{t_w^6}{2t_s^3} \left(\sum_{j=0}^3 \frac{a_3^{(j)}}{N_j (\pm t_s - E_{4M}^{(j)})} \right)^2, \end{aligned} \quad (\text{A10})$$

where we have now explicitly given a label to each of the four sets of a_j 's, and by extension, N_j 's as well. The \pm refers to the bonding and anti-bonding energy levels.

c. E_A Chain (green) Finally, the isolated atom chain has the following couplings

$$\begin{aligned} T_A &= -\frac{t_w^2}{2t_s}, \\ T_B &= -t_w^2 \sum_{j=0}^3 \frac{a_3^{(j)}}{N_j E_{4M}^{(j)}}. \end{aligned} \quad (\text{A11})$$

2. v_B cluster

For the v_B cluster's effective chains, we only have two categories, as shown in Fig. 13. The first (cyan) corresponds to a 4-atom molecular chain, with the same energy eigenvalues and eigenstates formulae as the previous ones, but with a different set of $\{t_b, t_s, t_w\}$ [see Eq. (8)]. The second (blue) subchain corresponds to the

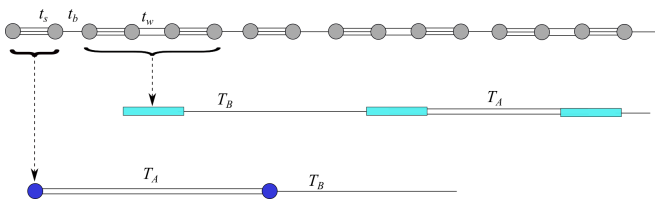


FIG. 13. Decimation of the v_B cluster's effective chain. The cyan rectangles represent the states corresponding to the four-atom molecules, like in Fig. 12. Below, we have the blue sites representing dimers, also similar to Fig. 12. The couplings in both cases follow a Fibonacci sequence and will also trifurcate after this step in the renormalization procedure.

2-atom molecular chain. We shall, once again, refer to them as the E_{4M} and E_{2M} chains, respectively.

a. E_{4M} Chain The couplings in this case are given by

$$\begin{aligned} T_A &= \frac{t_w}{N} a_3, \\ T_B &= \frac{a_3}{N} \frac{t_w^2 t_s}{E_{4M}^2 - t_s^2}. \end{aligned} \quad (\text{A12})$$

b. E_{2M} Chain The couplings for this chain are

$$\begin{aligned} T_A &= \pm \frac{t_w^2}{2} \sum_{j=0}^3 \frac{a_3^{(j)}}{N_j (\pm t_s - E_{4M}^{(j)})}, \\ T_B &= \pm \frac{t_w^3}{2} \left(\sum_{j=0}^3 \frac{a_3^{(j)}}{N_j (\pm t_s - E_{4M}^{(j)})} \right)^2. \end{aligned} \quad (\text{A13})$$

Appendix B: First-Order Energy Corrections of the Quasiperiodic Coupling scenario

E_0	E_1
v_A	$\frac{1}{\sqrt{2}} \sqrt{t_b^2 + 2t_s^2 + \sqrt{(t_b^2 + 2t_s^2)^2 - 4t_s^4}}$
	$\frac{1}{\sqrt{2}} \sqrt{t_b^2 + 2t_s^2 - \sqrt{(t_b^2 + 2t_s^2)^2 - 4t_s^4}}$
	t_s
	0
	$-t_s$
	$-\frac{1}{\sqrt{2}} \sqrt{t_b^2 + 2t_s^2 + \sqrt{(t_b^2 + 2t_s^2)^2 - 4t_s^4}}$
v_B	$\frac{1}{\sqrt{2}} \sqrt{t_b^2 + 2t_s^2 + \sqrt{(t_b^2 + 2t_s^2)^2 - 4t_s^4}}$
	$-\frac{1}{\sqrt{2}} \sqrt{t_b^2 + 2t_s^2 - \sqrt{(t_b^2 + 2t_s^2)^2 - 4t_s^4}}$
	t_s
	$-t_s$
	$-\frac{1}{\sqrt{2}} \sqrt{t_b^2 + 2t_s^2 + \sqrt{(t_b^2 + 2t_s^2)^2 - 4t_s^4}}$
	$-\frac{1}{\sqrt{2}} \sqrt{t_b^2 + 2t_s^2 - \sqrt{(t_b^2 + 2t_s^2)^2 - 4t_s^4}}$
$v_B + 2h$	t_s
	0
	$-t_s$

TABLE I. Nearest-order corrections to the three clusters v_A , v_B and $v_B + 2h$. Any next order correction will further split each of these energies into three, with corrections given by $\pm T_A$ and 0 (see Appendix A for the values of T_A in each case). Each of the three levels again will split into three and so on, with the well known spectrum structure of the hopping Fibonacci chain.